Numerical and Experimental Investigation of Single Point Incremental Forming Process for Phosphorus Bronze Hemispherical Cups

A. Chennakesava Reddy

Abstract— Incremental sheet forming (ISF) is a new technology employed for solving many problems from conventional sheet forming process in terms of more flexibility, inexpensive, short production time, suitable for small batches and especially rapid prototype production. The process is easily done on CNC machining centers with a rotating forming tool which moves along predefined trajectories that corresponds to the contour of the desired geometry. The present work was to investigate the finite element analysis of single point incremental sheet forming (SPIF) process to form hemispherical cups using phosphorous bronze alloy. ABAQUS 6.14 software code was used for finite element analysis. Experiments were carried on CNC machine and FEA results were validated with experimental results. The major SPIF process parameter which influences the formability of hemispherical cup was sheet thickness. The strains obtained through experimentation were within the limit of the formability limit diagram of phosphorus-bronze material.

Index Terms— Phosphorus bronze, incremental forming process, hemispherical cups.

1 Introduction

IN the incremental sheet forming (ISF), the universal spherical forming tool is moved along NC controlled tool path as follows: the tool moves down-wards, contacts the sheet, then draws a contour on the horizontal plane, and then makes a step downwards, draws next contour, next step downwards, and next contour and so on as shown in the figure 1. The process offers higher flexibility reducing the product development greatly and making it suitable for low volume production to fabricate 3D complex shapes.

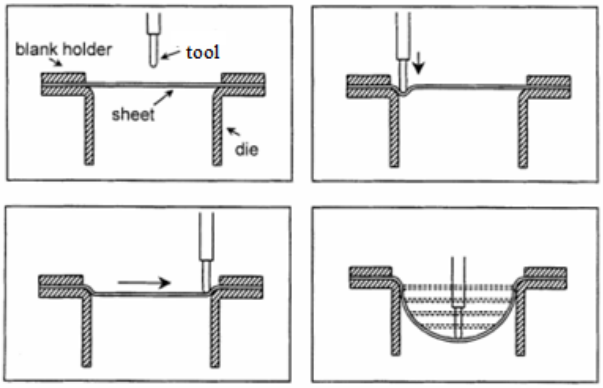

Fig. 1. Incremental sheet forming.

The techniques adopted for sheet metal operations in the olden days were pressing, spinning and deep drawing. In a series of research on deep drawing process, a rich investigation have been carried out on warm deep drawing process to improve the super plastic properties of materials such as AA1050 alloy [1], [2], [3], [4], [5,] [6], AA2014 alloy [7], AA2017 alloy [8], AA2024 alloy [9], AA2219 alloy [10], AA2618 alloy [11], AA3003 alloy [12], AA5052 alloy [13], AA5049 alloy [14], AA5052 alloy [15], AA6061 alloy [16], Ti-Al-4V alloy [17], EDD steel [18], gas cylinder steel [15].

In the recent years, many researchers worked in the field of incremental sheet forming. The effect of step depth, feed rate and diameter of the tool have been studied in cold incremental sheet forming of aluminum sheet [20], [21]. Kopac et al. [22] have given importance to the tool movement along the tool path, i.e tool path from center to the end of the sheet has good effect and also concluded that the optimal inclination of walls on the product are 45°, bigger angles may cause errors, cracks, and product failure. Tisza, et al. [23] have stated that due to the special incremental nature of deformation process, significantly higher deformation can be achieved compared to conventional sheet metal forming processes and it also follows from its unique deformation characteristics that materials with lower formability in conventional forming may be manufactured in an economic way. Azauzi et al. [24] have found that the forming forces depend largely on the proper design of the tool path. The forming force is slightly lower than the experimental values, but results are very good (Cerro et al. [25]). Forming forces obtained by numerical simulation show good correlation with measured values. However, it was a slight underestimation of the axial forces during thinning.

2 Materials and Methods

Phosphorous bronze sheet was used in this study of single point incremental sheet forming process. It is copper alloy containing the composition as 93.6-95.6%. Rest varies as given in Table 1. The addition of tin increases the corrosion resistance and strength of the alloy. The phosphorous increases the wear resistance and stiffness of the alloy. These alloys are notable for their toughness, strength, low coefficient of friction, and fine grain. Material properties considered in this study as

• *Alavala Chennakesava Reddy is currently Professor & Director (Foreign Relations) in JNT University, India, Mobile-09449568776. E-mail: chennakesava@jntuh.ac.in*

shown in Table 2 and imported to finite element analysis.

TABLE 1
COMPOSITION OF PHOSPHOROUS-BRONZE ALLOY

Fe	*Pb*	*P*	*Sn*	*Zn*
<=0.10%	*<=0.050%*	*0.030-0.35%*	*4.2-5.8%*	*<=0.30%*

TABLE 2
MECHANICAL PROPERTIES OF PHOSPHOROUS-BRONZE ALLOY

Density	*8860 kg/m3*
Yield strength	*380 MPa*
Poisson's ratio	*0.341*
Modulus of Elasticity	*110 GPa*

The values of true stress-true strain are taken from the tension test on the material Phosphorous bronze. Graph between stress and strain for phosphorous bronze is shown in figure 1. The obtained values were taken as material properties-plasticity for simulation of SPIF process. The values of true stress-true strain are taken from the tension test on the material Phosphorous bronze. Graph between stress and strain for phosphorous bronze is shown in figure 1. The obtained values were taken as material properties-plasticity for simulation of SPIF process.

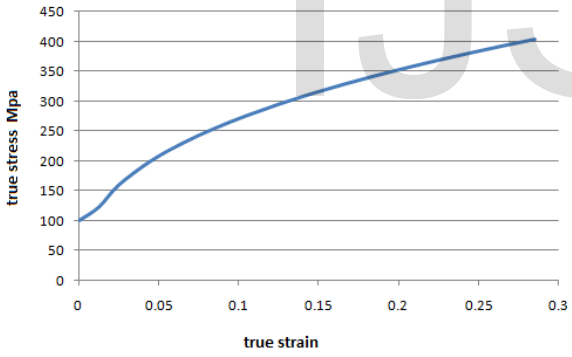

Fig. 1. True stress-strain curve of phosphorus-bronze.

2.1 Numerical Pre-processing

Pre-processing is represented schematically as shown in figure 2. A 150mm x 150 mm sheet as shown in figure 3, which is of deformable characteristic, was modeled. Tool for the experiment was designed with 6 mm radius. The tool was modeled as analytical rigid part. True stress-true strain experimental data were loaded in the tabular form as material properties. Contact is the interaction between tool and the sheet. The contact is modelled as frictional contact. Coefficient of friction was 0.15. Boundary conditions for the sheet and tool were given. For the sheet, all the four edges were fixed as show in figure 4. The boundary conditions for tool were four degrees of freedom, i.e linear movements in x, y and z directions and rotation about the axis of tool. The tool path generated from CAM software as shown in figure 5 was imported into the ABAQUS code and the simulation was run to optimize the parameters. Meshing is the process of discretizing the component. The sheet was meshed with S4R elements. S4R elements are uniformly reduced integration to avoid shear and membrane locking [26]. The element has several hourglass modes that may propagate over the mesh. Fine mesh gives the good results with greater computational time. Coarse mesh leads to inconsistent results, penetration and convergence problems during simulation process. A fine mesh of 2mm was generated for consistent results. The Table-3 shows the number of elements, nodes and variables produced after meshing the sheet. Meshed part is seen in the figure 6. Results were extracted from output database file generated by ABAQUS after the completion of FEA. von-Mises stress, strain rate and strains, sectional thickness, maximum principal strain, minimum principal strain were taken from output file for further analysis.

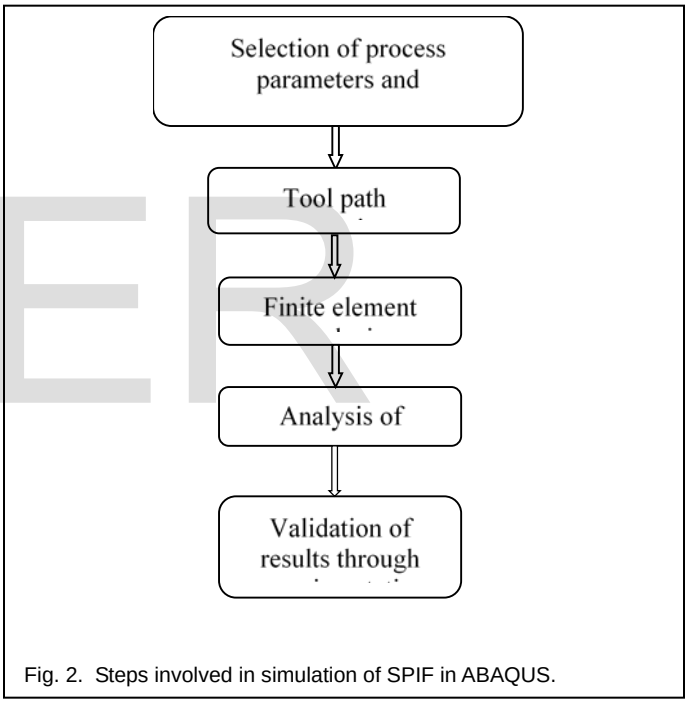

Fig. 2. Steps involved in simulation of SPIF in ABAQUS.

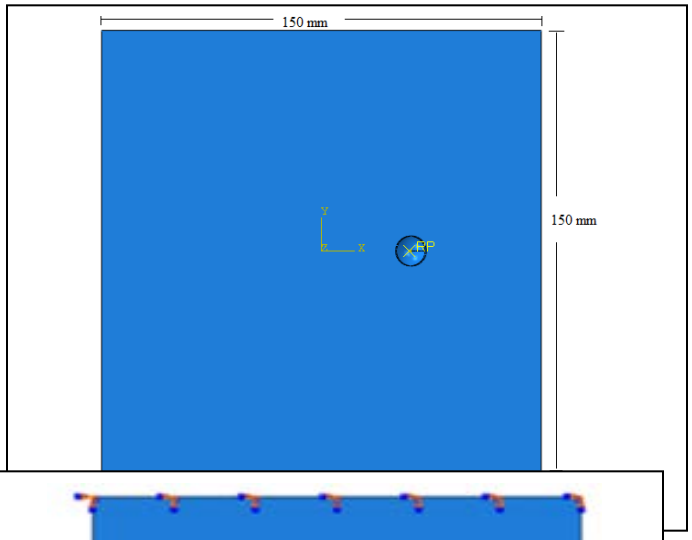

TABLE 3
NODES AND ELEMENTS

Element size	*2mm*
No. of Elements	*5625*
No. of Nodes	*5777*
Total no. of variables	*34662*

2.2 Experimental Validation

A 3-axis CNC machine was used in this work to perform SPIF process. The CNC machine consists of mainly 3 units they are machine tool, control unit and part program [27]. The part program is fed into machine control unit where it analyses the data. Then the control unit gives the commands for the movement of tool. Tool follows the set of instructions. Apart from these three units, sensors or feedback devices are also provided to check the errors.

In the present study, a sine wave CNC milling machine is used. It is a 3- axis machine. Table was given motions along X and Y directions. The tool which is fixed in spindle was rotated around its own axis and vertical motion was given along Z direction. Sheets of 150mm x 150mm are cut from the large sheet of thickness 1 and 1.2mm using the shearing machine. Holes are drilled on the corners of the sheet using drilling machine to hold firmly in the blank holder. Square patterns of 5mm distance (figure 7) are drawn on the two sheets for extracting the results from the finished part. Part program is a set of instructions written according to the required shape. Tool path for required shape is generated in CAM package and loaded in CNC machine. This sheet was mounted to the worktable of the CNC machine.

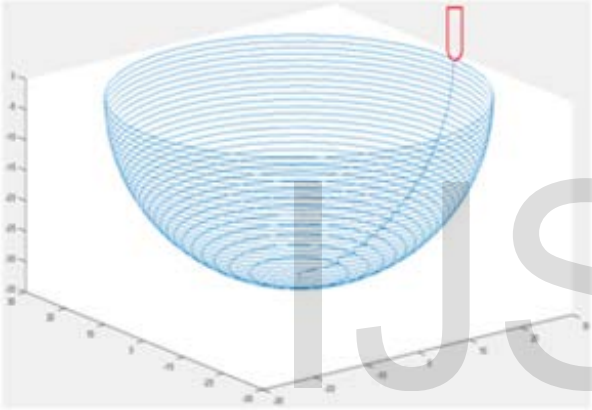

Fig. 5. Tool path generation.

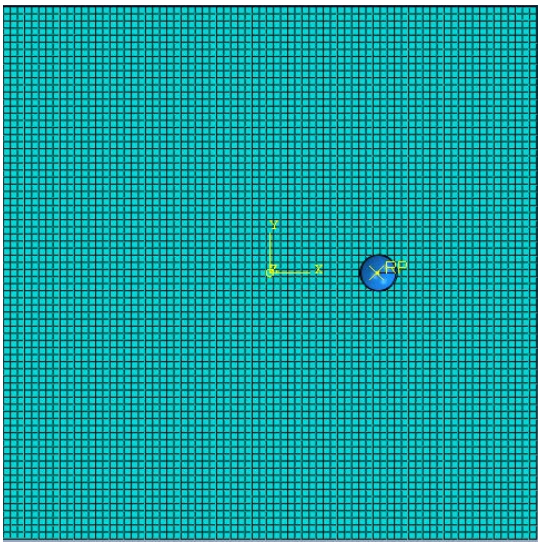

Fig. 6. Meshed part.

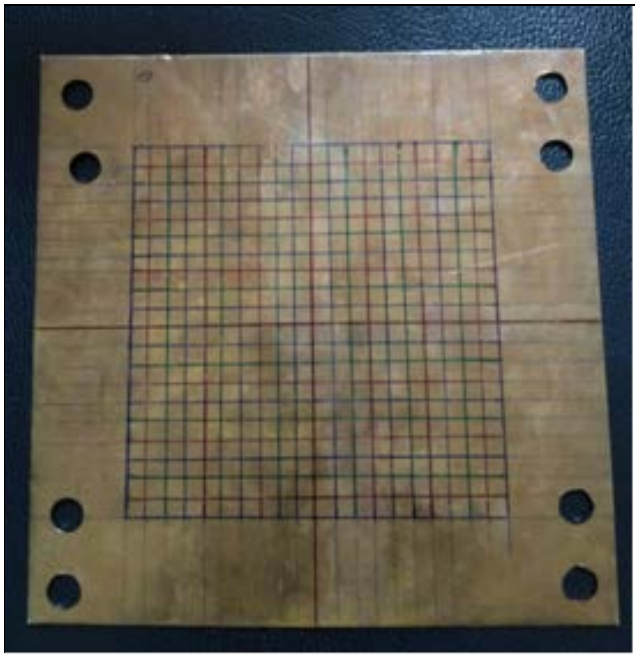

Fig. 7. Prepared sheet.

The clamping and top plates restrict flange material flow into the forming region that is defined by tool path generated from the CAM software and due to this clamping restriction tool applies much localized stresses to deform the sheet. Tool of 6 mm diameter was fixed in the tool holder. Before starting the experiment a demo run as shown in the figure 8, was done to check the errors. After completing the demo, the tool was set at specified position from centre using CNC controls. Program was initiated to start the forming. Lubricant was used at the interface of tool and work material. Figures 9 shows the formation of hemispherical cup and formed cup.

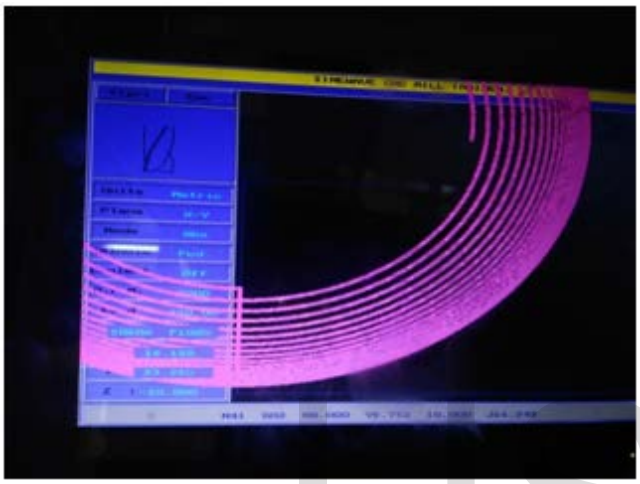

Fig. 8. Demo of CNC program on monitor screen.

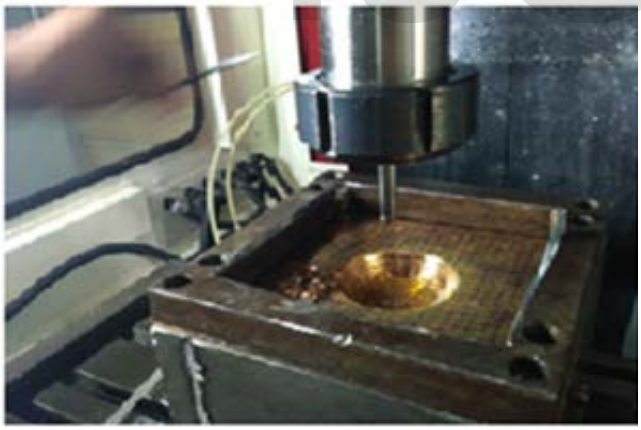

Fig. 9. Formed Hemispherical cup.

3 Results and Discussion

For 1mm and 1.2mm thick sheets the maximum equivalent stress induced are 365.8MPa and 361.0 MPa respectively as shown in the figures 10(a) and 10(b). For both the cups the maximum equivalent stress was found in the side walls of the cups. To validate the simulation results, the finite element grid of 5mm size was created on the backside of the cup material. The size of element was 2mm in case of simulation results. The stress and strain obtained by the finite element method coincides with the pattern on the cups. The stress patterns for formed cups of both 1 mm and 1.2 mm sheets are shown in the following figures 11(a) and 11(b), respectively.

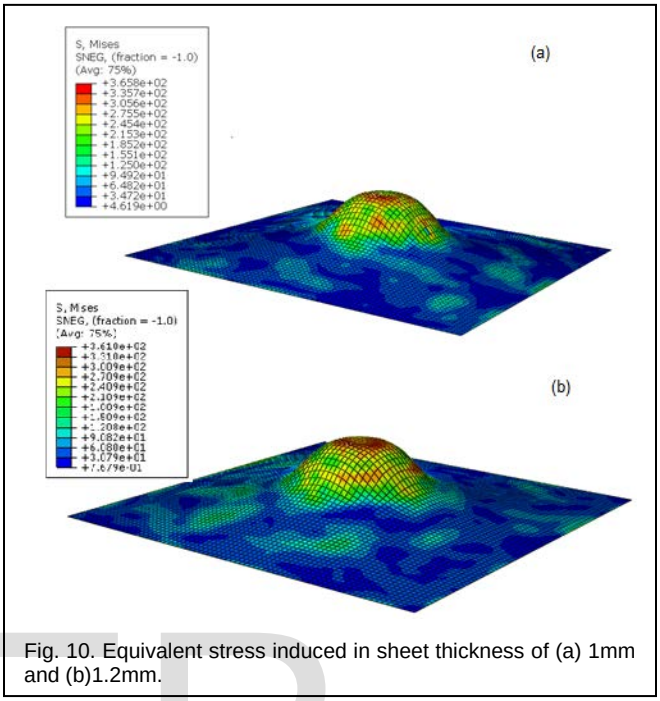

Fig. 10. Equivalent stress induced in sheet thickness of (a) 1mm and (b)1.2mm.

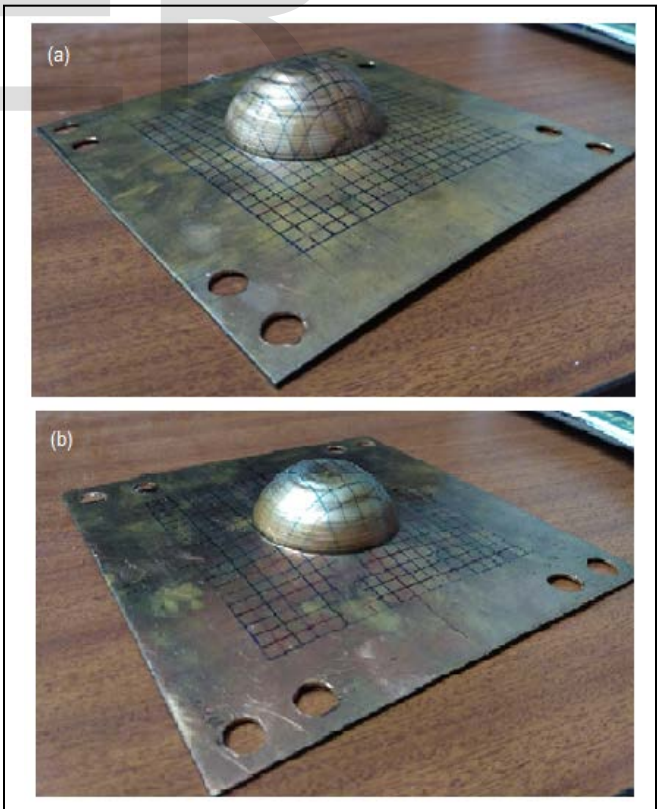

Fig. 11. Grid based deformation on hemispherical cup drawn on (a) 1mm sheet and (b) 1.2mm sheet.

The strains obtained from the experiment are in good agreement with the strains obtained from simulation. The strains obtained from the simulation for 1 mm and 1.2 mm sheets are 1.34 and 1.36, respectively, as shown in figures 12(a) and 12(b). Whereas the strains obtained from experimental are 1.1 and 1.2, respectively, figures 13 and 14. When comparing simulation strains with the experimental strains, the strains obtained from the experiment are found to be on the lower side. This is because of absence of fracture in the experimentally formed cups. The strains obtained from simulation are higher because they represent the maximum values of rupture. This further indicates experimental strains are within the allowable limits of the formability of cup.

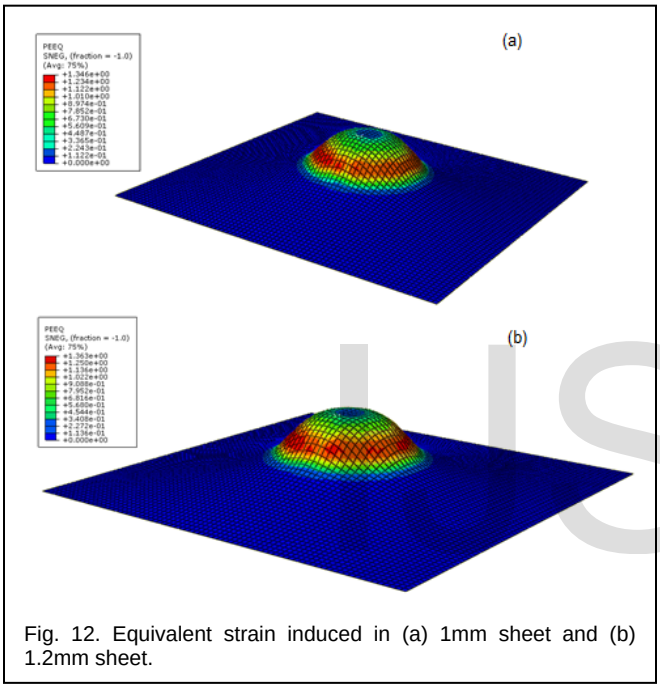

Fig. 12. Equivalent strain induced in (a) 1mm sheet and (b) 1.2mm sheet.

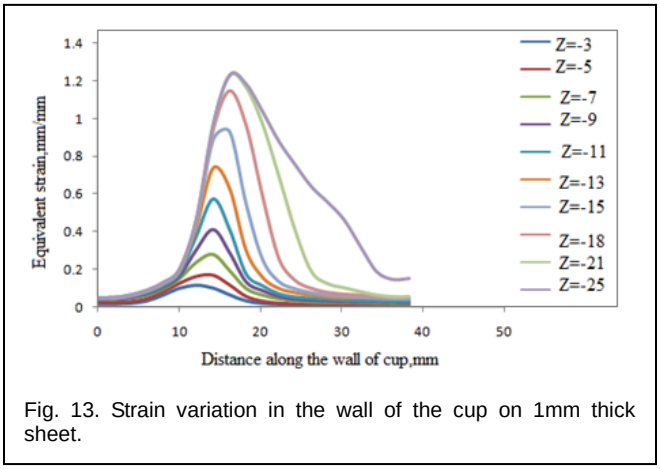

Fig. 13. Strain variation in the wall of the cup on 1mm thick sheet.

The strain variations along the walls of hemispherical cups are shown in figures 13 and 14, respectively. It is seen that in the initial stages of forming, the path of strain is almost linear and as the forming continues to take place the strain path follows a non-linear trend.

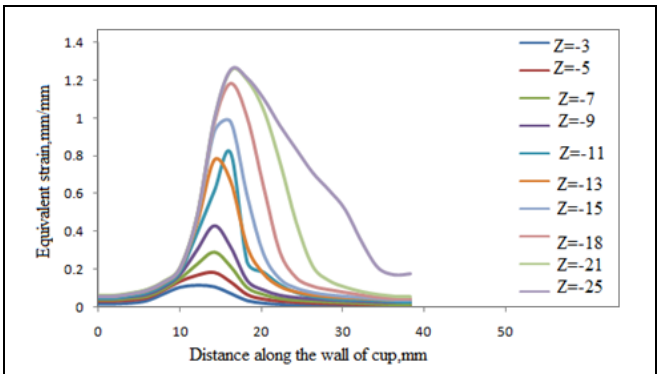

Fig. 14. Strain variation in the wall of the cup on 1.2mm thick sheet.

As observed from figure 15 the energy dissipated in the plane strain region is less than that dissipated in the shear lips. This is due to the higher stress triaxiality in this zone that favors the micro-mechanisms of damage.

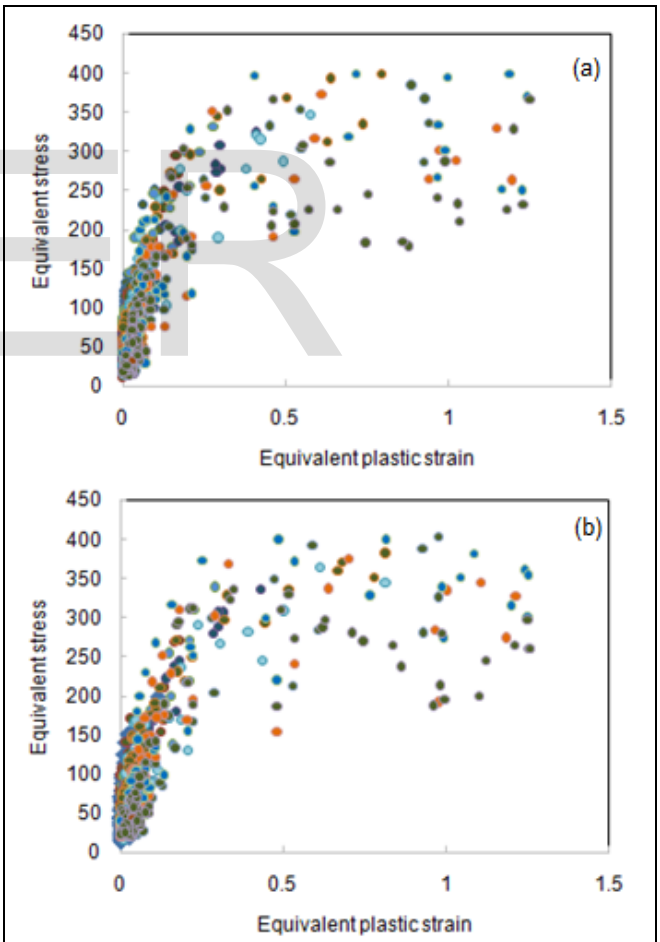

Fig. 15. Equivalent plastic strain vs equivalent stress for (a) 1mm and (b) 1.2mm thick sheets.

The thickness variations along the walls of cup for 1 mm and 1.2 mm sheets is shown in figures 16(a) and 16(b). The

thickness variation along the walls followed the same trend as predicted by the simulation. It is the side walls of the cups which experienced the maximum reduction in thickness. This is due to the reason that the side wall is the most strained part in the formed component. So, the elements in this part of the cup are more stretched when compare to other elements. The thickness reduction in the flange and the bottom of the cup was negligible.

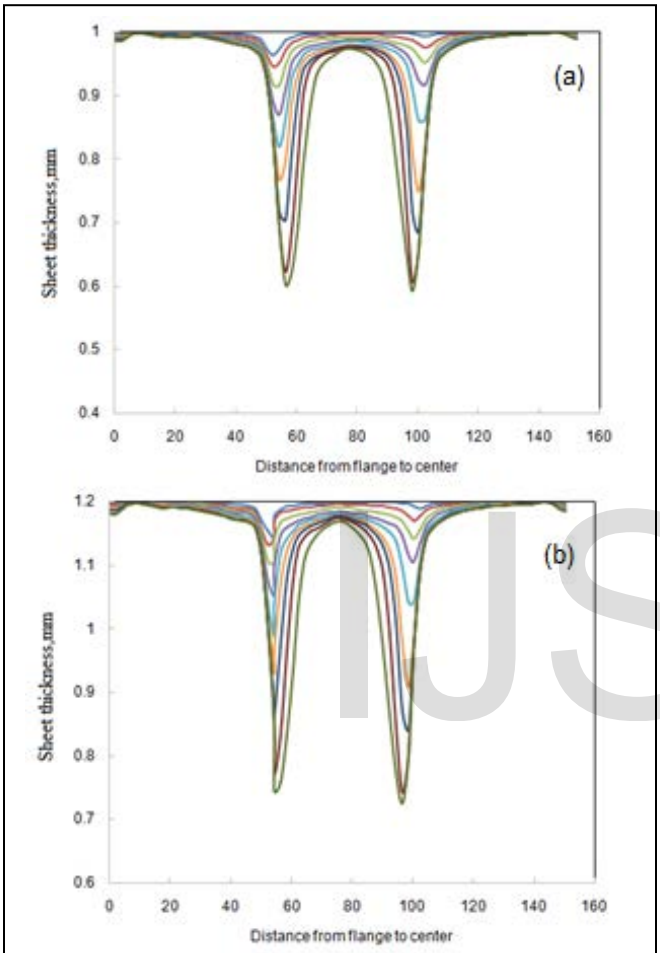

Fig. 16. Thickness variation along the walls of hemispherical cup for (a) 1mm and (b) 1.2mm thick sheets.

Figure 17 represents the formability diagrams for the 1 mm and 1.2 mm hemispherical cups. Both the cups follow the same pattern, which is; in the very initial stages of forming the compressive stresses are predominant. But in the later stages of forming the formability limit diagrams of both the cups are dominated by the uniaxial tensile stress.

4 Conclusion

In the present work, the finite element analysis and validation are successfully implemented for single point incremental forming process of phosphorous bronze sheet. The formability limit diagram was highly influenced by the sheet thickness. Experiments were conducted on CNC machine to verify the accuracy of simulated results. The experimental results were in good agreement with the simulated results. The stress pattern obtained on the formed cup was similar to that of the deformed pattern of mesh in simulated cups from FEA. The strain of the formed cup is within the limit of the formability curve.

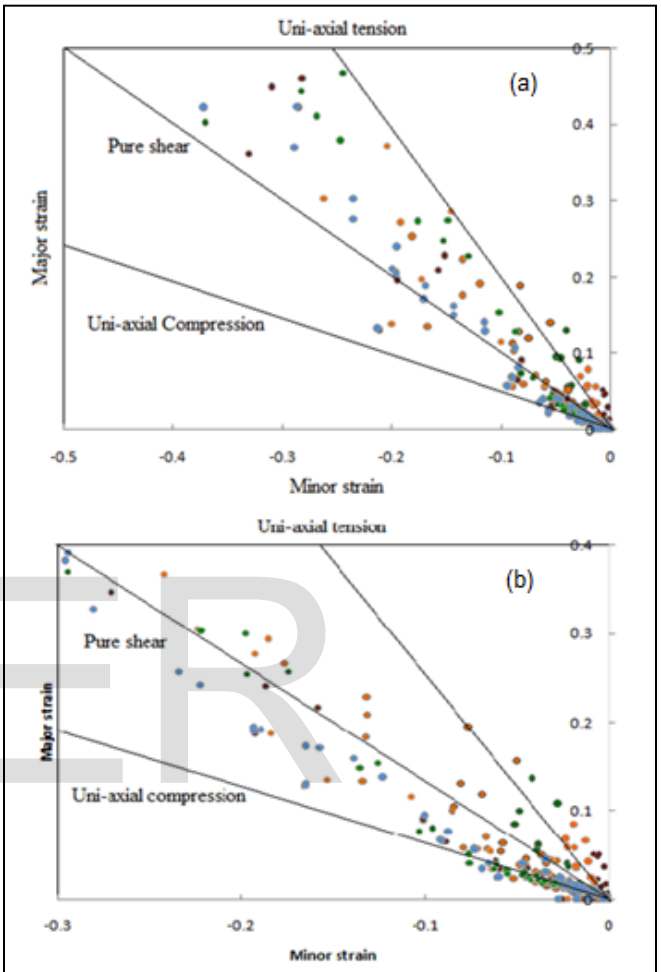

Fig. 17. Formability limit diagrams of (a) 1mm and (b) 1.2mm thick sheets.

Acknowledgment

The authors wish to thank UGC, New Delhi for financial assistance of this project.

References

[1] A. C. Reddy, Homogenization and Parametric Consequence of Warm Deep Drawing Process for 1050A Aluminum Alloy: Validation through FEA, International Journal of Science and Research, vol. 4, no. 4, pp. 2034-2042, 2015.
[2] A. C. Reddy, Formability of Warm Deep Drawing Process for AA1050-H18 Pyramidal Cups, International Journal of Science and Research, vol. 4, no. 7, pp. 2111-2119, 2015.
[3] A. C. Reddy, Formability of Warm Deep Drawing Process for AA1050-H18 Rectangular Cups, International Journal of Mechanical and Production Engineering Research and Development, vol. 5, no. 4, pp. 85-97, 2015.
[4] A. C. Reddy, Formability of superplastic deep drawing process with moving blank holder for AA1050-H18 conical cups, International Journal of Research in Engineering and Technology, vol. 4, no. 8, pp. 124-132, 2015.

[5] A. C. Reddy, Performance of Warm Deep Drawing Process for AA1050 Cylindrical Cups with and Without Blank Holding Force, International Journal of Scientific Research, vol. 4, no. 10, pp. 358-365, 2015.
[6] A. C. Reddy, Necessity of Strain Hardening to Augment Load Bearing Capacity of AA1050/AlN Nanocomposites, International Journal of Advanced Research, vol. 3, no. 6, pp. 1211-1219, 2015.
[7] A. C. Reddy, Parametric Optimization of Warm Deep Drawing Process of 2014T6 Aluminum Alloy Using FEA, International Journal of Scientific & Engineering Research, vol. 6, no. 5, pp. 1016-1024, 2015.
[8] A. C. Reddy, Finite Element Analysis of Warm Deep Drawing Process for 2017T4 Aluminum Alloy: Parametric Significance Using Taguchi Technique, International Journal of Advanced Research, vol. 3, no. 5, pp. 1247-1255, 2015.
[9] A. C. Reddy, Parametric Significance of Warm Drawing Process for 2024T4 Aluminum Alloy through FEA, International Journal of Science and Research, vol. 4, no. 5, pp. 2345-2351, 2015.
[10] A. C. Reddy, Formability of High Temperature and High Strain Rate Superplastic Deep Drawing Process for AA2219 Cylindrical Cups, International Journal of Advanced Research, vol. 3, no. 10, pp. 1016-1024, 2015.
[11] C. R Alavala, High temperature and high strain rate superplastic deep drawing process for AA2618 alloy cylindrical cups, International Journal of Scientific Engineering and Applied Science, vol. 2, no. 2, pp. 35-41, 2016.
[12] C. R Alavala, Practicability of High Temperature and High Strain Rate Superplastic Deep Drawing Process for AA3003 Alloy Cylindrical Cups, International Journal of Engineering Inventions, vol. 5, no. 3, pp. 16-23, 2016.
[13] C. R Alavala, High temperature and high strain rate superplastic deep drawing process for AA5049 alloy cylindrical cups, International Journal of Engineering Sciences & Research Technology, vol. 5, no. 2, pp. 261-268, 2016.
[14] C. R Alavala, Suitability of High Temperature and High Strain Rate Superplastic Deep Drawing Process for AA5052 Alloy, International Journal of Engineering and Advanced Research Technology, vol. 2, no. 3, pp. 11-14, 2016.
[15] C. R Alavala, Development of High Temperature and High Strain Rate Super Plastic Deep Drawing Process for 5656 Al- Alloy Cylindrical Cups, International Journal of Mechanical and Production Engineering, vol. 4, no. 10, pp. 187-193, 2016.
[16] C. R Alavala, Effect of Temperature, Strain Rate and Coefficient of Friction on Deep Drawing Process of 6061 Aluminum Alloy, International Journal of Mechanical Engineering, vol. 5, no. 6, pp. 11-24, 2016.
[17] A. C. Reddy, Finite element analysis of reverse superplastic blow forming of Ti-Al-4V alloy for optimized control of thickness variation using ABAQUS, Journal of Manufacturing Engineering, National Engineering College, vol. 1, no. 1, pp. 6-9, 2006.
[18] A. C. Reddy, T. Kishen Kumar Reddy, M. Vidya Sagar, Experimental characterization of warm deep drawing process for EDD steel, International Journal of Multidisciplinary Research & Advances in Engineering, vol. 4, no. 3, pp. 53-62, 2012.
[19] A. C. Reddy, Evaluation of local thinning during cup drawing of gas cylinder steel using isotropic criteria, International Journal of Engineering and Materials Sciences, vol. 5, no. 2, pp. 71-76, 2012.
[20] C. R Alavala, Fem Analysis of Single Point Incremental Forming Process and Validation with Grid-Based Experimental Deformation Analysis, International Journal of Mechanical Engineering, 5, 5, 1-6, 2016.
[21] C. R Alavala, Validation of Single Point Incremental Forming Process for Deep Drawn Pyramidal Cups Using Experimental Grid-Based Deformation, International Journal of Engineering Sciences & Research Technology, vol. 5, no. 8, pp. 481-488, 2016.
[22] J. Kopac and Z. Kampus, Incremental sheet metal forming on CNC milling machine-tool 13 International Science Conference on Achievement in Mechanical and materials Engineering, 2005.
[23] M. Tisza, General overview of sheet incremental forming, Journal of achievements in materials and Manufacturing Engineering, vol. 55, no. 1, pp. 113-120, 2012.
[24] M. Azaouzi, N. Lebaal, Tool path optimization for single point incremental sheet forming using response surface method, Simulation Modeling Practice Theory, vol. 24, pp. 49–58, 2012.
[25] I. Cerro, E. Maidagan, J. Arana, A. Rivero, P. P. Rodriguez, Theoretical and experimental analysis of the dieless incremental sheet forming process, Journal of Materilas Processing Technology,, vol. 177, pp. 404–408, 2006.
[26] C. R. Alavala, Finite element methods: Basic Concepts and Applications, PHI Learning Pvt. Ltd., 2008.
[27] C. R. Alavala, CAD/CAM: Concepts and Applications, PHI Learning Pvt. Ltd, 2008.